Research Article Vol. 13, No. 11 / 1 Nov 2023 / Optical Materials Express 3355
Optical Materials EXPRESS

Refractive index measurement of IP-S and IP-Dip photoresists at THz frequencies and validation via 3D photonic metamaterials made by direct laser writing

ELENA MAVRONA,[1,†] ANNA THEODOSI,[2,3,†] KRZYSZTOF MACKOSZ,[4] ELENI PERIVOLARI,[5] IVO UTKE,[4] JOHANN MICHLER,[4] JAKOB SCHWIEDRZIK,[4] MARIA KAFESAKI,[2,3] ODYSSEAS TSILIPAKOS,[6] AND ANGELOS XOMALIS[4,7,*]

[1]*Laboratory for Transport at Nanoscale Interfaces, Empa, Swiss Federal Laboratories for Materials Science and Technology, Dübendorf 8600, Switzerland*
[2]*Institute of Electronic Structure and Laser, Foundation for Research and Technology-Hellas, 70013, Heraklion, Crete, Greece*
[3]*Department of Materials Science and Technology, University of Crete, 70013, Heraklion, Crete, Greece*
[4]*Laboratory for Mechanics of Materials and Nanostructures, Empa, Swiss Federal Laboratories for Materials Science and Technology, Thun 3602, Switzerland*
[5]*Laboratory for Advanced Materials Processing, Empa, Swiss Federal Laboratories for Materials Science and Technology, Thun 3602, Switzerland*
[6]*Theoretical and Physical Chemistry Institute, National Hellenic Research Foundation, GR-11635 Athens, Greece*
[7]*Nanoelectronics and Photonics Group, Department of Electronic Systems, Norwegian University of Science and Technology, Trondheim 7034, Norway*
[†]Stands for equal contribution.
[*]*Angelos.Xomalis@ntnu.no*

Abstract: Direct laser writing (DLW) is widely used to fabricate complex metamaterials (MMs) and photonic devices for nanoscale applications across the electromagnetic frequency spectrum. While the optical properties of conventional photoresists used in DLW are well studied in the visible and infrared range, it is still unclear how they behave at lower frequencies. Here, we measure the refractive index and absorption of IP-S and IP-Dip photoresists within the THz range of the electromagnetic spectrum. Further, we utilize THz time-domain spectroscopy (THz-TDS) to experimentally measure the laser-processed three-dimensional (3D) MM structures. We conduct full-wave electromagnetic simulations using the measured refractive index values to validate our experiments. The THz-TDS measurements are in excellent agreement with the theoretical predictions verifying the validity of our refractive index measurements. This study aims to support and lead future investigations utilizing standard DLW photoresists for photonic applications in the THz range.

1. Introduction

The need for fast, large-area micro- and nano-fabrication techniques is ever-increasing and associated with a broad range of applications. Direct writing using ultrashort laser pulses is widely used for fabricating complex 3D multiscale structures for applications ranging from nano-optics to tissue engineering and catalysis [1–4]. This versatile, high-resolution fabrication process delivers structures with feature sizes from tens of nanometers to several millimeters [5,6].

#500287 https://doi.org/10.1364/OME.500287
Journal © 2023 Received 10 Jul 2023; revised 17 Aug 2023; accepted 17 Aug 2023; published 31 Oct 2023

Optical Materials EXPRESS

Metamaterial (MM) and metasurface-based devices have demonstrated immense potential for photonic applications due to their unique and unusual electromagnetic properties. Importantly, by varying the size of the constituent meta-atom (unit-cell), MM structures can operate across a vast range of frequencies, from microwaves up to THz and the visible spectrum [7–10]. While the dispersive refractive index $n(\omega)$ and absorption $a(\omega)$ of widely used photoresists in direct laser writing (DLW) are well-known and extensively characterized in the visible and the near-infrared range, it is not yet clear how they behave within the THz frequency range [11,12]. In the last decades, a rapid development of the infrared and THz science and technology has been witnessed [13,14]; thus, it is vital to carefully examine the properties of frequently used photoresists for nanofabrication within the THz range. As the refractive index of photosensitive materials is relatively low, photonic/optoelectronic devices usually require coating the polymeric scaffolds with different materials (metallic, metallic nanoparticles, semiconducting or denser dielectric materials) to reach the desired response [15–18]. In some cases, the coatings can be very thin, making the accurate simulation of the electromagnetic response of the composite structures a challenging task. Thus, there is a critical need for experimental characterisation of frequently used materials for nanofabrication to assist theoretical investigations of complex metamaterial designs.

Here, for the first time to our knowledge, we experimentally study the $n(\omega)$ and $a(\omega)$ of frequently used photoresists in the THz range. Subsequently, we utilize high-resolution, large-scale DLW (section 2.1) to fabricate 3D MMs, coat with atomic layer deposition (ALD, section 2.2) and measure their optical properties with THz time-domain spectroscopy (THz-TDS, section 2.3). Two important aspects distinguish this work from previous works on photoresists: firstly, their optical properties are fully-measured via THz-TDS for uncured, cured, and resists measured as thin films, and secondly as validation of our experiments on 3D printed dielectric metamaterials, we use the experimentally measured $n(\omega)$ and $a(\omega)$ to perform exact full-wave calculations in the THz range (section 2.4). The good agreement between simulations and experiment confirms the validity of our refractive index measurements. The reported optical properties of photosensitive materials can find extensive use by the photonics and MMs community.

In previous work, we consider two-layered structure, covered with metallic nanoparticles via electro-less plating for refractive index sensing applications at the mid-infrared transparency window [15]. By contrast, this work considers a multi-layer 3D structure (12 layers), coated with ZnO via atomic layer deposition (ALD) and is focused on the low THz frequency range.

2. Results and discussion

2.1. Direct laser writing (DLW)

3D THz structures were fabricated via DLW (Fig. 1(a)). Utilizing two-photon polymerization, DLW allows fabrication of high-resolution features far below the diffraction-limited laser spot size. Briefly, the beam of a near-infrared (NIR) pulsed laser is focused inside the volume of a negative tone photoresist (transparent in NIR range) tightly. Strong spatial confinement of the laser beam in combination with the ultrashort laser pulses (fs) causing the photo-initiator of the photoresist to absorb two or more photons and start the polymerisation locally resulting in structure resolution <100 nm. For our experiments, we use a conventional nanoprinter (Nanoscribe) with a Ti:Sapphire femtosecond (fs) laser at a center wavelength of 780 nm, 25 kW peak power, 100 fs pulse duration, and 80 MHz repetition rate. For achieving high-resolution features over large-size structures, essential for THz MMs measurements, we use a 25x magnification (0.8 NA, 3D MF) oil-immersion objective and IP-S photoresist (Nanoscribe) in dip-in laser lithography mode on standard THz transparent high resistivity Si wafers. With the aid of 3D sample stages and galvo mirrors, we fabricate 3D split cube resonator (SCR) MMs of about 3×3 mm^2 lateral size ($\sim 17 \times 17$ unit cells) and height of 700 µm. Scanning electron microscopy (SEM) images of the structure are depicted in Fig. 1(b), (d). Additional SEM images can be found in the Supplement

Optical Materials EXPRESS

1 (Fig. S2). The MMs smallest feature is approximately 13 µm. Following the fabrication, we apply a developing protocol consisting of PGMEA (30 min), isopropanol (5 min), and H_2O (single immersion) to wash off the unexposed photoresist.

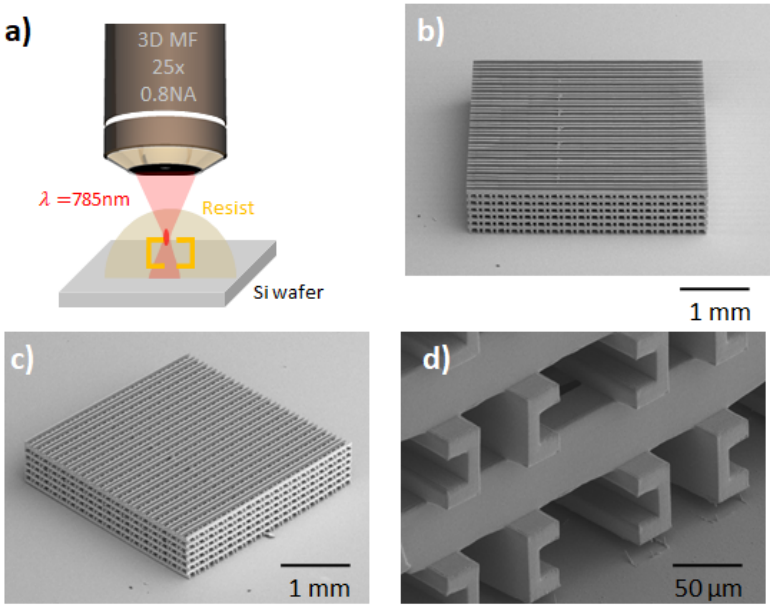

Fig. 1. Laser-processed THz mm-scale metamaterials (MMs). a) Direct laser writing (DLW) of 3D MMs. b-d) Scanning electron microscopy images of the split cube resonator (SCR) structure coated with 500 nm of ZnO via atomic layer deposition (ALD). In all cases, we use a λ = 785 nm fs laser, IP-S resist and Si wafer as a substrate.

2.2. *Atomic-layered deposition (ALD)*

Since the laser-processed polymeric scaffolds feature a relatively low $n(\omega)$, the sub-wavelength SCR meta-atom cannot support strong Mie-type resonances. As a result, as will become evident in the following section, the structure operates as a photonic crystal, and the spectral response is dominated by the corresponding bandgap. An approach to further enhance the light confinement properties of the SCR meta-atom is to apply a coating of denser dielectric material. We investigate this approach by depositing 500 nm of ZnO in a custom-built ALD system using diethyl zinc (DEZ) precursor and water (H2O) co-reactant at 50 degrees. Such lowering of the temperature (compared to standard ALD deposition temperatures of a few hundred of degrees) is achievable due to the high reactivity of DEZ. Moreover, the deposition parameters were 0.1 s for the precursor pulse, 1 s for exposure, and 90 s for the purge in both cases (DEZ and H2O). The precursor pulse and the purge were executed with 15 sccm and 100 sccm argon flows, respectively. Using SEM, we determine the thickness of the ZnO layer (500 nm, Fig. S3) and calculate the growth per cycle (GPC) of about 0.12 nm/cycle, allowing coating with extreme sub-nm resolution. The conformal coated structures show excellent mechanical and chemical stability, and dimensions are quite close to the desired ones.

2.3. *Refractive index of the resists and MMs measurements with THz time-domain spectroscopy (THz-TDS)*

For the optical characterization, we utilize a THz-TDS setup, which fully covers the frequency range of interest (0.45-1.50 THz). Briefly, the sample is placed on the rotation stage of the

Optical Materials EXPRESS

time-resolved THz spectrometer to allow normal light incidence (Tera Flash TF-1503, Toptica Photonics AG). The setup comprises a pair (before and after the sample position) of wire grid polarizers (G30X10-S, SEMIC RF) that allow polarization-resolved spectroscopy. Here THz pulses were collected in a data interval of about 70 ps with a resolution as high as 0.05 ps. For our measurements, a commercial system was used in ambient conditions. The beam size in the focus is 2 mm.

For the refractive index measurements, we used our previously suggested methodology considering thick sample approximation [19–21]. The THz transmission of a sample is calculated using a measurement of the sample ($E_{sample}(t)$) and a reference ($E_{ref}\ (t)$). The THz transmission

$$T_{exp}\,(\omega) = E_{sample}\,(\omega)\,/E_{ref}\,(\omega) \tag{1}$$

is given then by the Fourier transforms of the THz electric field of the reference ($E_{ref}\ (\omega)$) and the sample $E_{sample}(\omega)$. The calculation of the THz transmission is used for the characterization of the 3D THz MM but also for the extraction algorithm of the complex refractive index

$$\tilde{n} = n + \iota\kappa \tag{2}$$

of the photoresists in the THz regime. For the refractive index extraction, the experimental value of the THz transmission ($T_{exp}(\omega)$) is fitted with a theoretical transmission based on the propagation and Fresnel formulas ($T_{theo}(\omega)$). For the fitting, the numerical method Newton Raphson, is used. Here, the only unknown parameter is the complex refractive index which is calculated using the fitting of the experimental transmission ($T_{exp}(\omega)$) and the theoretical transmission ($T_{theo}(\omega)$). In all cases, we measured the samples, before and after curing, using THz-TDS. As the photoresists were in the liquid phase (blue lines, Fig. 2), we placed them between two windows of cyclic olefin copolymer (TOPAS, highly transparent in the THz range) with thicknesses of 2 mm [22]. The windows were glued together using epoxy with spacers with a thickness of about 0.5 mm. Further, the thicknesses of the samples were carefully measured using a micrometer and the optical properties were extracted using a standard parameter extraction algorithm as described previously [20]. After the UV curing of the samples, they were measured again using the same THz-TDS apparatus (red lines, Fig. 2). For clarity, we removed the TOPAS windows and measured the cured photoresist films (yellow lines, Fig. 2).

The quantities measured and depicted in Fig. 2 are the real part of the refractive index $n(\omega)$ and the intensity attenuation coefficient $a(\omega)$, connected with the extinction coefficient ($\kappa(\omega)$, the imaginary part of the complex refractive index) through

$$a(\omega) = 2\kappa(\omega)\omega/c \tag{3}$$

IP-S shows a relatively spectrally-constant $n(\omega)$ (blue, Fig. 2(a)) that changes slightly upon curing and when measured as a cured film. IP-S $a(\omega)$ exhibits a fairly linear increase in all cases from 10 to 40 cm^{-1} for the frequency range between 0.40-1.50 THz (Fig. 2(c)). Further, uncured IP-Dip shows higher $n(\omega)$ of about 1.75 that is reduced to 1.63 after the resist is cured (0.40 THz, Fig. 2(b)). Similarly, the absorption of the IP-Dip reaches 60 cm^{-1} at around 1.50 THz. This drops to 40 cm^{-1} for the cured and film samples at 1.50 THz (Fig. 2(d)). Recent studies focused on commercially available photoresists indicate similar refractive index of the cured IP-S highlighting the validity of our measurements [23,24]. Further detailed measurements of such photoresists show now that absorption can be decreased by 5x times at the THz range as well as fabrication directly on thin films leading to highly conformable metasurfaces.

As mentioned earlier, for validating the $n(\omega)$ and $a(\omega)$ measurements, we fabricate a 3D SCR MM structure via DLW and using IP-S as photoresist, which is ideal for the fabrication of such structure sizes. Due to the low $n(\omega)$ of the polymer scaffold and the relatively thin ZnO coating (compared to the excitation wavelength), the structure is anticipated to act as a

Optical Materials EXPRESS

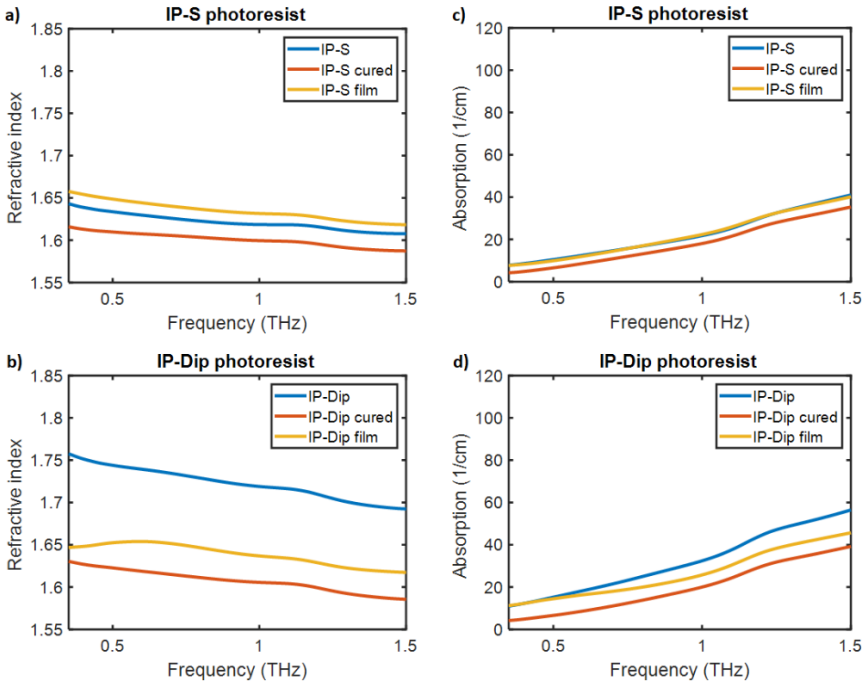

Fig. 2. Measured dispersive refractive index $n(\omega)$ and absorption $a(\omega)$ of IP-S and IP-Dip at the THz range. a-b) $n(\omega)$ and c-d) $a(\omega)$ measurements of IP-S and IP-Dip photoresists. In all cases, blue, red, and yellow stand for uncured, cured, and resists measured as cured thin films.

photonic crystal exhibiting a bandgap. In other words, any resonance of the sub-wavelength SCR meta-atom would manifest at higher frequencies compared to the bandgap. The dimensions of the structure are selected in such a way that the bandgap resides at the desired THz range. The aim is to reproduce with full-wave simulations the optical response of the THz structure using the experimentally measured $n(\omega)$ and $a(\omega)$ (see next section). To ensure that incoming radiation only excites the MM structure, we added an iris in the excitation path resulting in a spot size of approximately 2 mm. The linear polarization direction is controlled by either the rotation of the sample stage or the polarizer's relative angle. Linearly polarized light along the y-axis is exciting the free-standing structure (Si is removed) and collected with a THz detector in the back. The iris helps to minimize measurement noise due to air.

The measurements are depicted in Fig. 3. A clear bandgap is found near 1 THz that partially blocks (due to the limited number of layers along the z-axis) transmission through the structure. In addition, a trend for decreasing transmission through the structure is witnessed as the frequency increases.

2.4. Electromagnetic simulations

To verify the experimental results, we conduct full-wave calculations for the SCR MMs using the measured $n(\omega)$ and $a(\omega)$ of IP-S. From the $a(\omega)$ coefficient, we can extract the imaginary part of the refractive index (κ) using the formula

$$\kappa(\omega) = \alpha(\omega)\lambda_0/(4\pi), \tag{4}$$

where λ_0 is the free-space wavelength.

Optical Materials EXPRESS

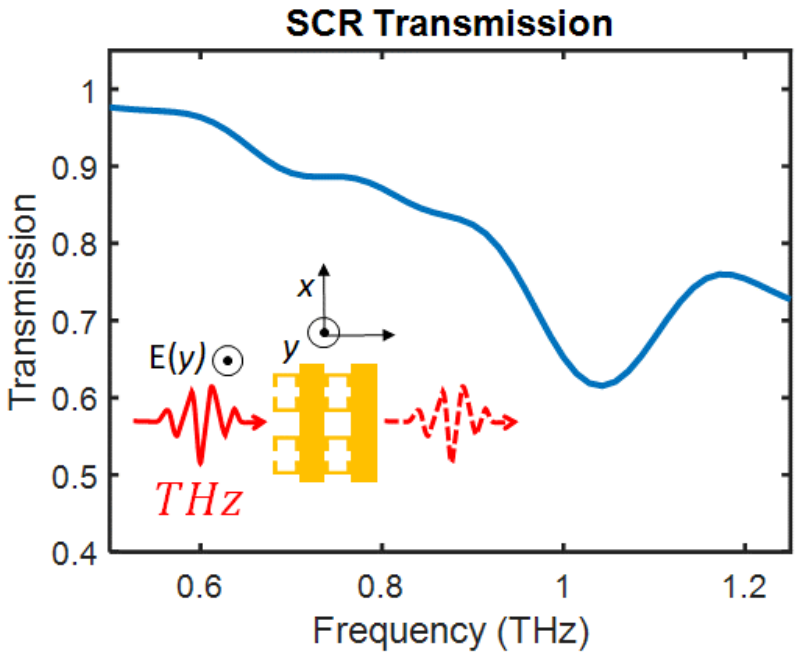

Fig. 3. Experimental transmission measurements of 3D THz MM. Normalized transmission of the free-standing SCR MM structure, see inset (twelve layers of SCRs are present in the sample, for simplicity we show only four). The IP-S polymer scaffold is conformally coated with 500 nm of ZnO via ALD.

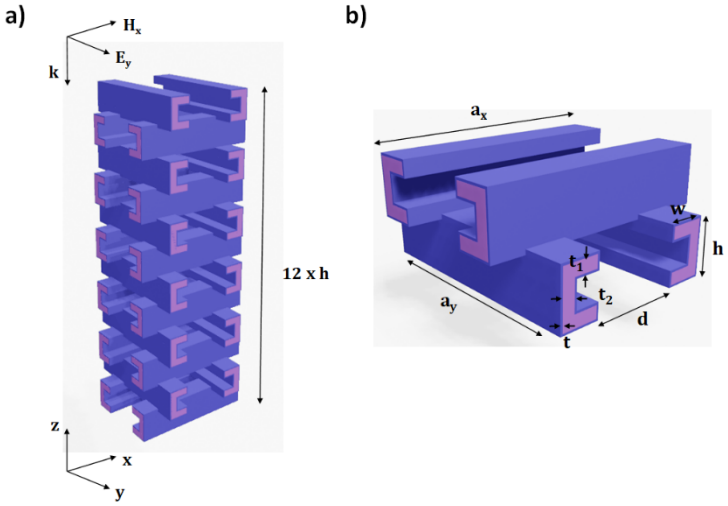

Fig. 4. Structure of split-cube-resonator (SCR) metamaterial. (a) Structure used for simulations, composed of twelve layers of SCRs. (b) Unit-cell of the periodic structure with annotated geometrical parameters.

We use the frequency-domain solver of the commercial software CST Studio based on the finite element method considering an unstructured mesh comprised of tetrahedra, as is typical for this method. We initially specify that the largest dimension of any tetrahedron of the mesh

Optical Materials EXPRESS

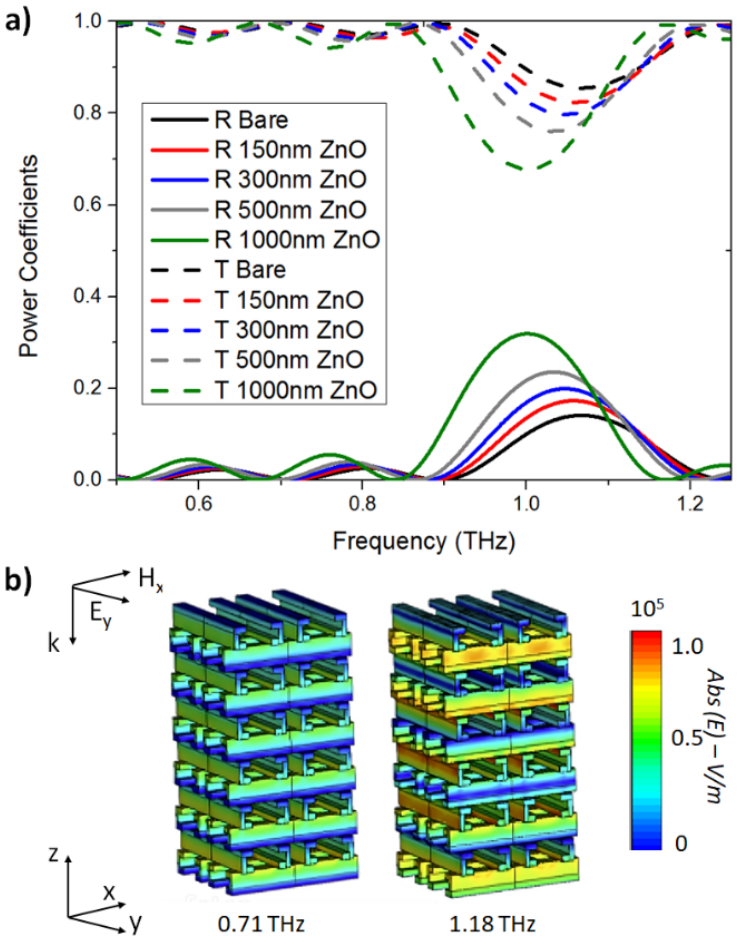

Fig. 5. Simulation results for bare and ZnO-coated THz MMs. a) Reflection (solid) and transmission (dashed) power coefficients of uncoated (black) and 150 nm (red), 300 nm (blue), 500 nm (grey) and 1000 nm (green) ZnO-coated SCR MMs. In all cases, we consider ZnO as lossless. (b) Field distributions for the bare MM structure at around the bandgap frequency (right) and at a frequency below the bandgap (below). A sharp difference in the degree of light localisation in the structure is clearly visible.

should not exceed λ/10. Subsequently, the mesh is automatically refined through the "adaptive mesh refinement" option, until the desired accuracy (convergence) is achieved. This typically means that in the final mesh smaller tetrahedra are found in domains requiring finer meshing, such as the 80-nm-thick ZnO coating, whereas, in domains such as top and bottom air domains, a sparser mesh is used. The entire procedure is automatic and results in an optimal mesh saving computer time and guaranteeing convergence of the result. More specifically, the final mesh will be selected after the "S-parameter termination criterion" is met, meaning that the computed S-parameters (reflection/transmission coefficients) have converged (the error among consecutive calculations with different meshes drops below a predefined limit, which is set to 1%). Further, simulations are performed on a structure composed of twelve layers of SCRs (z-axis) with periodic boundary conditions at the x and y axes, as depicted in Fig. 4(a), with the in-plane lattice constants $a_x = a_y = 186\ \mu m$. The bandgap of the photonic crystal is formed due to the

Optical Materials EXPRESS

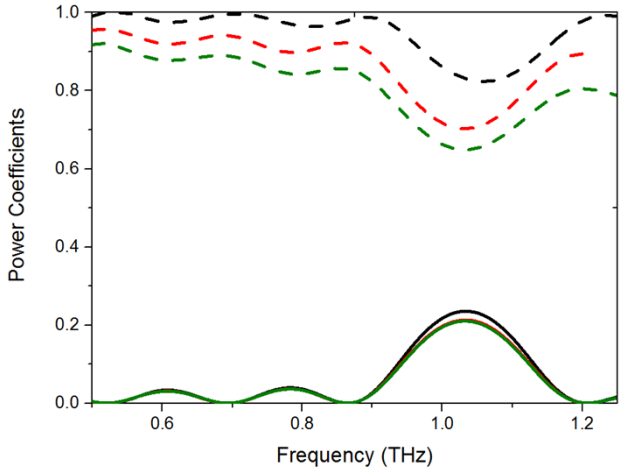

Fig. 6. Simulation results for ZnO-coated THz MMs with a coating thickness of 500 nm, as in the experiment (Fig. 3). Reflection (solid) and transmission (dashed) power coefficients for 7.29 (black), $7.29 + 0.5i$ (red), and $7.29 + 1.0i$ (green) ZnO permittivity.

periodic repetition of the SCR layers along the z-axis. As we increase the number of layers along the z direction, the bandgap deepens (see Fig. S1 in Supplement 1).

A single SCR has the following dimensions: $h = 60\ \mu$m, $w = 33\ \mu$m, $t_1 = 16.5\ \mu$m and $t_2 = 12\ \mu$m with reference to Fig. 4(b). The SCRs are placed in pairs of two facing each other at a distance $d = 75\ \mu m$. Then, the next SCR layer is rotated by 90° in a woodpile-style fashion (Fig. 4(b)). This two-layer structure constitutes the unit cell of the periodic system (Fig. 4(b)), which upon periodic repetition results in the full structure (Fig. 4(a)). The structure is excited by a linearly polarized plane wave that propagates along the z axis, and we obtain both reflected and transmitted power coefficients.

First, we focus on the uncoated SCR. Reflection and transmission (power coefficients) are depicted in Fig. 5(a) with black solid and dashed curves, respectively. The bandgap appears near 1 THz. Characteristic field distributions at the bandgap frequency and at a frequency below the bandgap are depicted in Fig. 5(b). A sharp difference in the degree of light localisation in the structure is clearly visible, as anticipated. Next, the coated structure is investigated by progressively considering 150-, 300-, 500- and 1000-nm thick ZnO coatings. As the coating thickens, the bandgap deepens due to the stronger refractive index contrast. In addition, we observe a redshift of the bandgap center frequency, coming from the increased average refractive index of the SCR "particles". In all cases, though, the bandgap is found near 1 THz, in agreement with the experimental results (Fig. 3).

However, unlike the experimental data, our simulations show a relatively constant transmission level outside the forbidden band (compare Fig. 3 and 5(a)). To investigate the possible nature of this discrepancy, we repeat the simulations, but this time with different values of the imaginary part of the ZnO electric permittivity (to account for losses of the coating). More specifically, the electric permittivity

$$\varepsilon_r = \varepsilon' + \varepsilon'' i \tag{5}$$

is assumed (based on previous experimental measurements) equal to 7.29 (black lines, Fig. 6), $7.29 + 0.5i$ (red), and $7.29 + 1.0i$ (green) [25]. Here, the ZnO coating thickness has been set to 500 nm as in the experiment. As the imaginary part increases, a fairly linear drop in the overall transmission level appears, which seems to match better our experimental measurements (see blue line in Fig. 3 and green dashed line in Fig. 6).

Optical Materials EXPRESS

3. Summary

We have measured, for the first time to the best of our knowledge, the dispersive refractive index and absorption of frequently used IP-S and IP-Dip photoresists at the THz frequency range. This provides new possibilities for predicting the behavior of THz photonic devices. Two important features distinguish this work from previous works on photoresists: we have fabricated dielectric 3D MM structures with DLW, and compared the experimentally measured response (THz-TDS) against full-wave simulations, adopting the measured refractive index and absorption data. Our simulation results verify the THz-TDs data, highlighting the validity of the refractive index measurements. Further investigations may concern assembling a refractive index and absorption library of frequently used photoresists or other materials used for 3D printing at the THz range. The acquired properties of widely used photoresists should be effective in providing guidance for predicting and accurately simulating the electromagnetic response of complex 3D printed MM and photonic structures at THz frequencies.

Funding. Hellenic Foundation for Research and Innovation (916); Eidgenössische Materialprüfungs- und Forschungsan stalt (IRC 2021).

Acknowledgments. The authors would like to acknowledge the support of the company TOPAS Advanced Polymers GmbH for providing TOPAS substrate.

Disclosures. The authors declare no conflicts of interest.

Data availability. All data used for the figures are available upon reasonable request from the corresponding author.

Supplemental document. See Supplement 1 for supporting content. Regarding the dependence of number of layers along the z direction and bandgap as well as SEM images of the ZnO coating thickness.

References

1. B. Buchegger, J. Kreutzer, B. Plochberger, R. Wollhofen, D. Sivun, J. Jacak, G. J. Schütz, U. Schubert, and T. A. Klar, "Stimulated emission depletion lithography with mercapto-functional polymers," ACS Nano **10**(2), 1954–1959 (2016).
2. A. Selimis, V. Mironov, and M. Farsari, "Direct laser writing: Principles and materials for scaffold 3D printing," Microelectron. Eng. **132**, 83–89 (2015).
3. N. Anscombe, "Direct laser writing," Nat. Photonics **4**(1), 22–23 (2010).
4. S. McGee, Y. Lei, J. Goff, C. J. Wilkinson, N. N. Nova, C. M. Kindle, F. Zhang, K. Fujisawa, E. Dimitrov, and S. B. Sinnott, "Single-step direct laser writing of multimetal oxygen evolution catalysts from liquid precursors," ACS Nano **15**(6), 9796–9807 (2021).
5. V. Hahn, T. Messer, N. M. Bojanowski, E. R. Curticean, I. Wacker, R. R. Schröder, E. Blasco, and M. Wegener, "Two-step absorption instead of two-photon absorption in 3D nanoprinting," Nat. Photonics **15**(12), 932–938 (2021).
6. M. Manousidaki, D. G. Papazoglou, M. Farsari, and S. Tzortzakis, "Abruptly autofocusing beams enable advanced multiscale photo-polymerization," Optica **3**(5), 525–530 (2016).
7. N. Engheta and R. W. Ziolkowski, *Metamaterials: Physics and Engineering Explorations* (John Wiley & Sons, 2006).
8. C. M. Soukoulis and M. Wegener, "Past achievements and future challenges in the development of three-dimensional photonic metamaterials," Nat. Photonics **5**(9), 523–530 (2011).
9. S. B. Glybovski, S. A. Tretyakov, P. A. Belov, Y. S. Kivshar, and C. R. Simovski, "Metasurfaces: From microwaves to visible," Phys. Rep. **634**, 1–72 (2016).
10. D. Zografopoulos and O. Tsilipakos, "Recent advances in strongly-resonant and gradient all-dielectric metasurfaces," Mater. Adv. **4**(1), 11–34 (2023).
11. M. Schmid, D. Ludescher, and H. Giessen, "Optical properties of photoresists for femtosecond 3D printing: refractive index, extinction, luminescence-dose dependence, aging, heat treatment and comparison between 1-photon and 2-photon exposure," Opt. Mater. Express **9**(12), 4564–4577 (2019).
12. T. Gissibl, S. Wagner, J. Sykora, M. Schmid, and H. Giessen, "Refractive index measurements of photo-resists for three-dimensional direct laser writing," Opt. Mater. Express **7**(7), 2293–2298 (2017).
13. A. Xomalis, X. Zheng, R. Chikkaraddy, Z. Koczor-Benda, E. Miele, E. Rosta, G. A. Vandenbosch, A. Martínez, and J. J. Baumberg, "Detecting mid-infrared light by molecular frequency upconversion in dual-wavelength nanoantennas," Science **374**(6572), 1268–1271 (2021).
14. J. Shi, D. Yoo, F. Vidal-Codina, C.-W. Baik, K.-S. Cho, N.-C. Nguyen, H. Utzat, J. Han, A. M. Lindenberg, and V. Bulović, "A room-temperature polarization-sensitive CMOS terahertz camera based on quantum-dot-enhanced terahertz-to-visible photon upconversion," Nat. Nanotechnol. **17**(12), 1288–1293 (2022).
15. A. Xomalis, O. Tsilipakos, M. Manousidaki, O. Pérez De Gregorio Busquets, G. Kenanakis, S. Tzortzakis, M. Farsari, C. M. Soukoulis, E. N. Economou, and M. Kafesaki, "Enhanced refractive index sensing with direction-selective three-dimensional infrared metamaterials," ACS Appl. Opt. Mater. **1**(1), 10–16 (2023).

Optical Materials EXPRESS

16. H. Mei, W. Yang, X. Zhao, L. Yao, Y. Yao, C. Chen, and L. Cheng, "In-situ growth of SiC nanowires/carbon nanotubes on 3D printed metamaterial structures to enhance electromagnetic wave absorption," Mater. Des. **197**, 109271 (2021).
17. S. Ghosh and S. Lim, "Perforated lightweight broadband metamaterial absorber based on 3-D printed honeycomb," Antennas Wirel. Propag. Lett. **17**(12), 2379–2383 (2018).
18. A. Jaiswal, S. Rani, G. P. Singh, T. Archana, M. Hassan, A. Nasrin, V. G. Gomes, S. Saxena, and S. Shukla, "Carbon quantum initiators enabled direct laser writing: A technique for fabrication of dielectric, all-carbon chiral metasurfaces," Carbon **208**, 43–49 (2023).
19. E. Mavrona, Y. Hu, G. D. F. Siqueira, M. Rüggeberg, S. Popov, L. A. Berglund, E. Hack, G. Nyström, and P. Zolliker, "Efficiency assessment of wood and cellulose-based optical elements for terahertz waves," Opt. Mater. Express **13**(1), 92–103 (2023).
20. E. Mavrona, U. Chodorow, M. Barnes, J. Parka, N. Palka, S. Saitzek, J.-F. Blach, V. Apostolopoulos, and M. Kaczmarek, "Refractive indices and birefringence of hybrid liquid crystal-nanoparticles composite materials in the terahertz region," AIP Adv. **5**(7), 077143 (2015).
21. D. Zwyssig, E. Hack, P. Zolliker, and E. Mavrona, "3D printed microfluidic devices using TOPAS filament for THz spectroscopic measurements," Opt. Mater. Express **13**(4), 1031–1040 (2023).
22. E. Mavrona, J. Graf, E. Hack, and P. Zolliker, "Optimized 3D printing of THz waveguides with cyclic olefin copolymer," Opt. Mater. Express **11**(8), 2495–2504 (2021).
23. E. J. Y. Magaway, Y. Farahi, S. M. Hanham, Z. J. Zhang, A. Guaidía-Moreno, and M. Navarro-Cía, "Silica nanoparticle-based photoresin for THz high-resolution 3D microfabrication by two-photon polymerization," IEEE Transactions on Terahertz Science and Technology **13**, 077143 (2023).
24. A. Ottomaniello, P. Vezio, O. Tricinci, F. M. Den Hoed, P. Dean, A. Tredicucci, and V. Mattoli, "Highly conformable terahertz metasurface absorbers via two-photon polymerization on polymeric ultra-thin films," Nanophotonics **12**(8), 1557–1570 (2023).
25. Y. Kim, J. Ahn, B. G. Kim, and D.-S. Yee, "Terahertz birefringence in zinc oxide," Jpn. J. Appl. Phys. **50**(3R), 030203 (2011).